Review of Scientific Instruments ARTICLE pubs.aip.org/aip/rsi

Quantitative determination of lateral spatial resolution in confocal Raman microscopy using graphene cross-edge scanning

Cite as: Rev. Sci. Instrum. 97, 023702 (2026); doi: 10.1063/5.0302635
Submitted: 16 September 2025 • Accepted: 25 January 2026 •
Published Online: 18 February 2026

Zhong-Jie Wang,[1,2] Tao Liu,[1,2] Xue-Lu Liu,[1,2] Miao-Ling Lin,[1,2] and Ping-Heng Tan[1,2,a)]

AFFILIATIONS

[1] State Key Laboratory of Semiconductor Physics and Chip Technologies, Institute of Semiconductors, Chinese Academy of Sciences, Beijing 100083, China
[2] Center of Materials Science and Optoelectronics Engineering, University of Chinese Academy of Sciences, Beijing 100049, China

[a)] **Author to whom correspondence should be addressed:** phtan@semi.ac.cn

ABSTRACT

Lateral spatial resolution (LSR) is a key parameter of confocal Raman microscopy, determining the system′s ability to resolve fine structural and chemical details at micro- to nanoscales. This study introduces a quantitative method to determine the LSR of a confocal Raman microscope using cross-edge one-dimensional Raman scan measurements of the area-sensitive G mode and edge-length-sensitive D mode intensity profiles at graphene edges. The measured LSR values for an objective with numerical aperture (NA) of 0.90 approach diffraction-limited estimates when the pinhole size is close to zero; however, LSR measurements with large confocal apertures yield values significantly larger than diffraction-limited predictions, as confirmed by measurements across objectives with varying NAs (NA = 0.25–0.90). The results demonstrate that achieving optimal resolution requires precise laser focusing, appropriate pinhole size selection, and beam expansion matching the objective′s entrance pupil, while defocusing or reduced beam diameter degrades performance. This method provides a practical and quantitative approach for LSR evaluation in confocal Raman microscopy, applicable to diverse experimental conditions.

I. INTRODUCTION

Confocal Raman spectroscopy is a powerful analytical technique widely employed for material characterization.[1–3] A key performance metric of such systems is lateral spatial resolution (LSR), i.e., the minimum distinguishable distance between two adjacent points in the x-y plane. The LSR fundamentally governs the system′s ability to resolve fine morphology details and directly impacts the accuracy of spectral data acquisition and imaging capabilities on the sample surface at micro- and nano-scales.[4–20] High LSR enables the discrimination of fine structural differences, as well as precise detection of localized variations in chemical composition,[21] molecular orientation,[22] and structural defects,[11,12,23] as well as localized physical phenomena such as strain distribution,[24] and phase transitions.[25] These factors often govern the functional properties of advanced materials. In Raman imaging, insufficient LSR can result in signal averaging across heterogeneous regions, obscuring critical details and compromising data reliability. Therefore, developing quantitative LSR evaluation methods is essential not only for ensuring robust experimental results but also for supporting theoretical modeling and advancing next-generation devices.[26]

In a non-confocal Raman microscope (where the pinhole is sufficiently large), the LSR is fundamentally determined by the system's ability to distinguish two closely spaced point sources as separate features in the image plane. This diffraction-limited resolution is quantitatively described by the Rayleigh criterion,

$$\mathrm{LSR}_{\mathrm{non-cf}} = \frac{0.61\lambda_{\mathrm{ex}}}{NA}, \tag{1}$$

where λ_{ex} is the excitation wavelength and NA is the numerical aperture of the objective. In contrast, for a confocal Raman microscope equipped with a point detector and operating at identical excitation and detection wavelengths ($\lambda_{\mathrm{ex}} = \lambda_{\mathrm{dt}}$), the diffraction-limited lateral

resolution is approximately improved by a factor of $\sqrt{2}$ compared to the conventional Rayleigh limit (i.e., the minimum resolvable distance is reduced by $\sqrt{2}$).[27] For the general case of a confocal Raman microscope with different excitation and detection wavelengths ($\lambda_{ex} \neq \lambda_{dt}$), the diffraction-limited LSR can be expressed as[27]

$$\mathrm{LSR}_{cf} = \frac{1}{\sqrt{1+\beta^2}} \cdot \frac{0.61\lambda_{ex}}{NA}, \quad (2)$$

where $\beta = \lambda_{ex}/\lambda_{dt}$. These relationships indicate that shorter excitation wavelengths and higher numerical aperture objectives generally yield better (smaller) LSR values. However, it is important to emphasize that Raman microscopy involves more complex optical processes. Effects such as the scattering of laser and Raman photons and the optical interactions at sample interfaces can degrade the practically achievable resolution. Moreover, experimental factors, including the focal depth, variations in the beam diameter during measurements, and the choice of confocal aperture size, may further influence the effective LSR under real-world conditions.

Several approaches have been proposed to evaluate the LSR value in Raman microscopy. A common approach employs reference samples with sub-diffraction-limited features, such as carbon nanotubes,[6,14,28] localized crystal defects,[10] gold nano-lines,[15] and nanoparticles,[18] where the spatial spread of their Raman signals serves as an LSR benchmark. Although straightforward, this technique requires reference materials with strong Raman contrast and precisely defined dimensions. In addition, practical limitations arise from sample preparation challenges and the need for sparsely distributed, isolated features. A more widely used alternative is the knife-edge method,[29,30] in which the laser beam (used for Raman excitation) is scanned across a sharp material edge while analyzing the intensity profile to determine the effective spot size. This approach benefits from not requiring specialized calibration samples and can be performed under standard experimental conditions. However, this method is susceptible to edge-related artifacts, including signal distortions and localized enhancements,[31–33] which may compromise both LSR modeling and measurement accuracy. Consequently, developing a simple, robust, and reliable method for LSR determination in Raman spectroscopy is essential to overcome current limitations.

The Raman intensity from a bulk crystal primarily originates from a region comparable to the optical penetration depth, leading to wavelength-dependent, edge-related artifacts in the spectral profile. In contrast, single-layer graphene (1LG) possesses atomic-scale thickness; thus, Raman artifacts associated with edges in bulk crystals, such as signal distortion and localized enhancement,[31–33] are absent at 1LG edges. More importantly, transverse optical phonons near the K point at one-dimensional armchair edges can be activated via a double-resonance scattering process, giving rise to the characteristic D mode in the Raman spectrum. A cross-edge 1D Raman scan of the D mode directly corresponds to the line spread function of the confocal Raman microscope, providing a directly measurable one-dimensional blur profile[13] that encapsulates the system′s imaging performance for LSR.

In this study, we introduce a quantitative method to determine the LSR in confocal Raman microscopy using cross-edge 1D Raman scan measurements at the edge of 1LG on a 90-nm SiO_2/Si substrate. By modeling the laser beam as a Gaussian profile, we derived analytical expressions for Raman intensity as a function of laser position near the 1LG edge, thereby clearly distinguishing the edge-length-sensitive D mode from the area-sensitive G mode. We validate our approach by demonstrating that the consistent LSR values obtained from both modes using NA = 0.90 are close to the diffraction-limited theoretical LSR when the pinhole size is near zero. In addition, we investigate the impact of pinhole size, focal depth, and beam diameter variations on the measured LSR, emphasizing the critical role of selection of the confocal aperture size, proper laser focusing, and laser beam expanding for optimal system performance. This work provides a simple yet quantitative framework for evaluating LSR under practical measurement conditions, along with actionable insights for enhancing Raman imaging system performance.

II. EXPERIMENTAL METHODS

The 1LG flake was mechanically exfoliated from bulk crystals and directly deposited onto a 90-nm SiO_2/Si substrate, providing sufficient optical contrast to allow both the 1LG flake and its edges to be clearly identified under an optical microscope. Raman spectroscopy was performed in a backscattering configuration using a Horiba HR800 confocal Raman microscope equipped with an edge filter and a charge-coupled device (CCD) detector. The confocal pinhole size of this system can be automatically adjusted within a range of 0–160 μm. Room-temperature spectra were acquired using four objectives: a 100× (NA = 0.90), two 50× (NA = 0.75 and 0.45), and a 20× (NA = 0.25). Excitation was provided by a 532 nm diode-pumped solid-state laser (output power: 40 mW). The power delivered to the sample was reduced to ~0.5 mW, measured below the objective, to minimize laser-induced heating.[34] Beam expanders of varying magnifications were used to adjust the laser spot size. Proper focusing on the graphene plane was achieved by performing a z axis scan to maximize the intensity of the G mode, which is a sensitive and reliable indicator of optimal focal position for 1LG. For the one-dimensional cross-edge Raman scan profile of the G and D modes near the 1LG edge, two scanning stages of SCANplus 75 × 50 (Märzhäuser Wetzlar GmbH & Co. KG) and P-733.2CD (Physik Instrumente SE & Co. KG) were employed to achieve step sizes of 0.1 and 0.025 μm, respectively. These step sizes were verified using a stage micrometer. The peak area was used to model the intensity profile.

III. THEORETICAL MODEL

The intensity distribution of the laser beam is essential to analyze LSR of confocal Raman microscopy. We model the laser beam as a Gaussian beam because it accurately represents the fundamental transverse mode emitted by most lasers. This mode exhibits a smooth, radially symmetric intensity profile that minimizes diffraction effects and allows for the tightest possible focusing, a critical requirement for achieving high spatial resolution in applications such as confocal Raman microscopy. Figure 1(a) depicts the vertical and horizon cross sections of the Gaussian beam. In the focal plane ($z = 0$), the intensity distribution of Gaussian beam I^{GB} reaches the peak at center and gradually decreases away from the center, following the equation:[35]

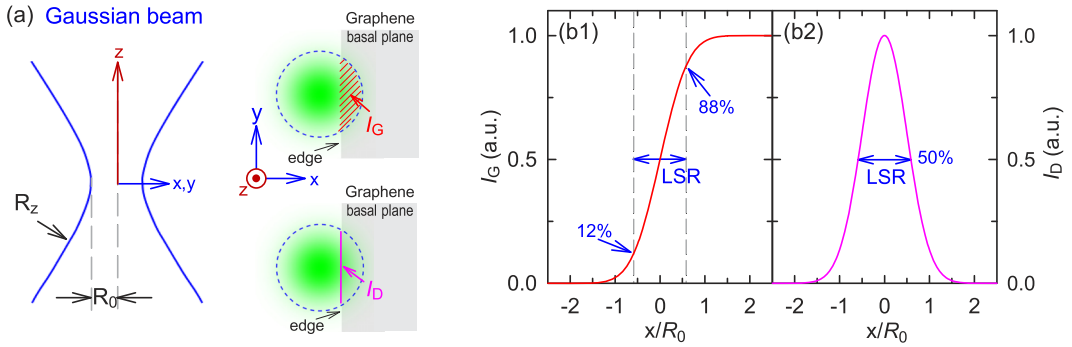

FIG. 1. (a) Vertical and horizontal cross sections of a Gaussian laser beam, illustrating the area and edge length contributions to the area-sensitive and edge-length-sensitive Raman intensity of 1LG, respectively. (b) Normalized I_G (b1) and I_D (b2) as functions of x/R_0.

$$I^{GB}(x',y') = I_0 \exp\left(-\frac{2\left((x'-x)^2+(y'-y)^2\right)}{R_0^2}\right), \quad (3)$$

where I_0 is the intensity of the laser beam center, (x',y') are the coordinates of any point in the focal plane and (x,y) are the coordinates of the laser beam center. The beam waist radius (R_0) at $z = 0$ of a Gaussian laser beam is defined as the distance between the center and the position where I^{GB} is the $1/e^2$ of I_0.

The G mode in 1LG arises from the first-order Raman scattering of zone-center E_{2g} optical phonon. Due to the atomic-scale thickness of 1LG, the G mode intensity (I_G) is sensitive to the laser-illuminated area. In contrast, the D mode intensity (I_D) depends primarily on the length of the illuminated edge. When a Gaussian laser beam with a beam waist radius R_0 is scanned perpendicularly across the 1LG edge in a 1D measurement, both I_G and I_D are further modulated by the spatial intensity distribution of the beam across their respective sensitive dimensions, i.e., area for I_G and edge length for I_D, as follows:

$$I_G(x) \propto \frac{2}{\sqrt{2\pi}R_0}\int_0^{+\infty} \exp\left(-\frac{2(x'-x)^2}{R_0^2}\right)dx', \quad (4)$$

$$I_D(x) \propto \exp\left(-\frac{2x^2}{R_0^2}\right), \quad (5)$$

where x is the distance from the 1LG edge.

Figures 1(b1) and 1(b2) present the normalized I_G and I_D profiles, respectively, calculated from Eqs. (4) and (5), plotted as functions of the normalized position x/R_0. The I_G profile exhibits a characteristic sigmoidal shape. In contrast, the I_D profile closely follows a Gaussian distribution with a full width at half maximum (FWHM) of $\sqrt{2\ln 2}R_0$. By fitting the experimental I_G and I_D profiles to Eqs. (4) and (5), respectively, the parameter R_0 can be determined, which corresponds to the Gaussian laser beam's spot size at the sample surface. Notably, the I_D profile directly represents the line spread function of the confocal Raman microscope. The experimental LSR (LSR_{exp}) derived from the I_D profile is equal to its FWHM [as indicated by the double-headed arrow in Fig. 1(b2)], i.e., $\sqrt{2\ln 2}R_0$. The I_G profile follows the behavior expected from the knife-edge method.[13] Consequently, the standard straight-edge method defined by ISO 18516:2019[36] can be applied for LSRexp determination using the I_G profile, where the LSR_{exp} is defined as the distance between the 12% and 88% relative intensity points on the sigmoidal I_G profile [Fig. 1(b1)].

IV. RESULTS AND DISCUSSION

To validate the aforementioned method, we performed Raman measurements on an exfoliated 1LG flake from natural graphite. An optical image of the flake is shown in Fig. 2(a), where the armchair and zigzag edges are indicated. The monolayer nature of the 1LG flake deposited on the SiO_2/Si substrate is confirmed by the single Lorentzian lineshape of its 2D mode,[37] which indicates negligible interaction between the 1LG and the substrate for the purpose of Raman analysis. The presence or absence of the D mode in the Raman spectrum acquired at the 1LG edge serves to identify the edge chirality. As demonstrated in Fig. 2(b), the absence of a D mode identifies a zigzag edge, while its distinct presence indicates armchair character,[38] consistent with the double-resonance Raman scattering mechanism.

We performed cross-edge 1D Raman scan measurements at an armchair edge of 1LG using a 532 nm excitation in the $\bar{z}(yy)z$ backscattering geometry.[39] In this configuration, the polarizations of both the incident and scattered light are aligned parallel to the graphene edge, with the edge itself oriented along the laboratory y axis. Figure 2(c) shows a schematic of the measurement location at the armchair edge. The corresponding I_G and I_D profiles, measured with a step size of 0.1 μm under the highest spatial resolution conditions (NA = 0.90, pinhole = 20 μm), are presented in Figs. 2(d1) and 2(d2), respectively, as functions of the lateral distance x from the edge. The I_G profile exhibits the sigmoidal shape predicted in Fig. 1(b1), while the I_D profile follows a Gaussian-like curve consistent with Fig. 1(b2). Fitting the I_G profile with Eq. (4) and the I_D profile with Eq. (5) yields experimental lateral spatial resolution (LSR_{exp}) values of 0.28 ± 0.02 and 0.27 ± 0.01 μm, respectively. For the measurements with a finer step size of 0.025 μm under the same optical conditions (NA = 0.90, pinhole = 20 μm), the resulting I_G and I_D profiles are shown in Figs. 2(e1) and 2(e2), respectively. Fitting the two profiles yields the same LSR_{exp} value of 0.27 ± 0.01 μm. These

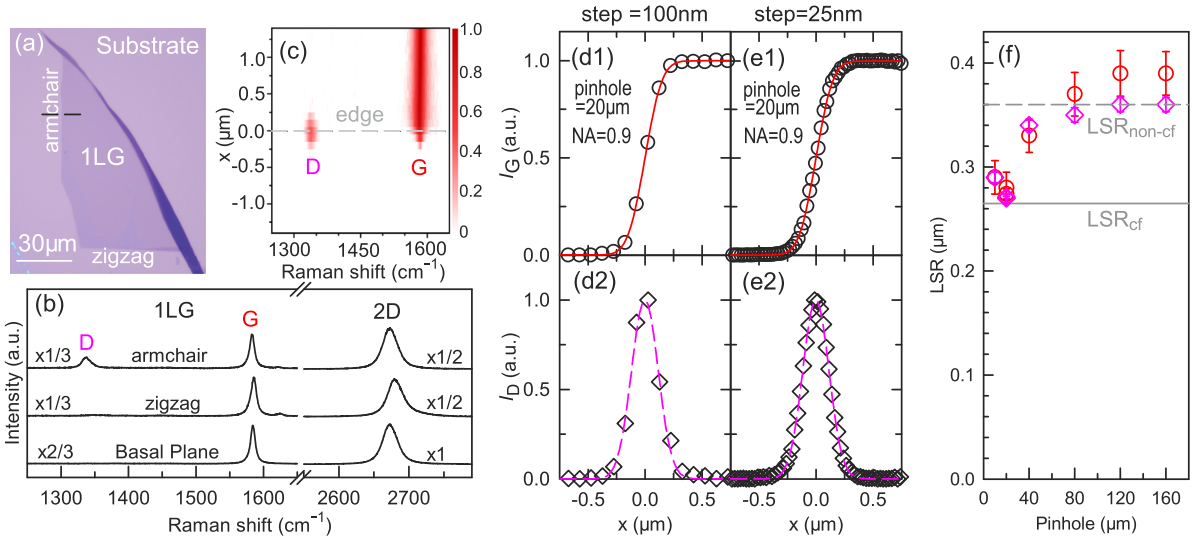

FIG. 2. (a) Optical image of the 1LG flake with its armchair and zigzag edges indicated. (b) Raman spectra acquired from the basal plane, armchair edge, and zigzag edge of the 1LG flake. (c) 1D Raman scan across the 1LG armchair edge. (d1 and e1) I_G and (d2 and e2) I_D intensity profiles as functions of distance from the armchair edge, measured using an objective with NA = 0.90 and a pinhole size of 20 μm. The open circles represent experimental data; the solid and dashed lines are fitted curves based on Eqs. (4) and (5). The step sizes are 0.1 μm for (d1 and d2) and 0.025 μm for (e1 and e2). (f) LSR$_{exp}$ as a function of pinhole size, derived from 1D cross-edge Raman scan of the D (open diamonds) and G (open circles) modes as well as LSR$_{non\text{-}cf}$ (gray dashed line) and LSR$_{cf}$ (gray solid line).

results are consistent with each other and in excellent agreement with the diffraction-limited estimate for a confocal Raman microscope, LSR$_{cf}$, calculated using Eq. (2) [gray solid line in Fig. 2(f)]. Furthermore, systematic measurements with a step size of 0.1 μm across pinhole sizes from 10 to 160 μm [Fig. 2(f)] show that LSR$_{exp}$ increases with aperture size. For instance, at a pinhole size of 80 μm, the extracted LSR$_{exp}$ values (0.35 μm from I_G and 0.37 μm from I_D) align well with the diffraction-limited estimate for a non-confocal Raman microscope, LSR$_{non\text{-}cf}$, given by Eq. (1) (gray dashed line). This non-confocal value is ~30% larger than that for the confocal case, which is attributed to the enlarged aperture collecting Raman signal from a broader area beyond the confocal resolution limit. It should be noted that the larger uncertainty associated with the G band primarily results from the limited number of data points across the edge transition region, as well as from additional intensity variations within the 0/plateau regions (both interior and exterior to the flake), as also illustrated in Fig. 3.

To quantitatively reveal the effect of NA on LSR, cross-edge 1D Raman scan measurements were performed using four objectives (NA = 0.9, 0.75, 0.45, and 0.25) with a pinhole size of 80 μm, and the I_G and I_D profiles as functions of edge distance x are depicted in Figs. 3(a) and 3(b), respectively. The I_G profile exhibits a less sharp

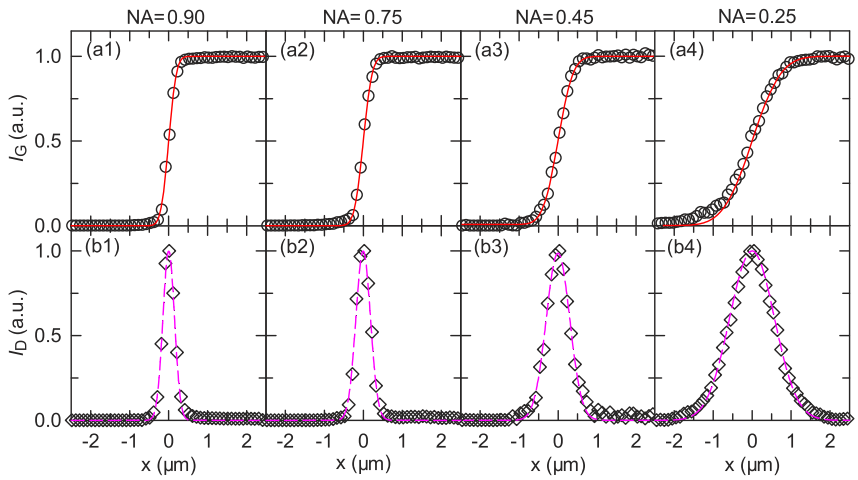

FIG. 3. (a) I_G and (b) I_D at the 1LG armchair edge as functions of edge distance, measured using four objectives with NA = 0.90, 0.75, 0.45, and 0.25, where the open circles/diamonds denote the experimental data and the solid/dashed lines represent the fitted curves based on Eqs. (4) and (5).

gradient near the edge at lower NA, with lower NA values resulting in larger LSR_{exp} (Table I). The FWHM of the I_D profile broadens with decreasing NA. For objectives measured with a pinhole size of 80 μm, the resulting LSR_{exp} was significantly larger (by >30%) than the confocal limit LSR_{cf} predicted by Eq. (2). This indicates that a pinhole size of 80 μm is too large for the system to operate in a diffraction-limited, strictly confocal regime. Nevertheless, this aperture size remains practically useful, as it effectively blocks the pervasive fluorescent background generated by photo-excited delocalized carriers, thereby improving the signal-to-noise ratio of the Raman signal.[40]

When the laser focal plane is misaligned with the sample surface by Δz, the projected spot size corresponds to the Gaussian beam waist at Δz, which expands with increasing Δz as follows:[35]

$$R_{\Delta z} = R_0\sqrt{1+\left(\frac{\Delta z\lambda_{ex}}{\pi R_0^2}\right)^2}. \quad (6)$$

This will cause the measured LSR_{exp} to deviate from the value obtained at the best focus on the sample surface. Figure 4 compares the I_G and I_D profiles near the 1LG edge for different Δz up to 0.6 μm (NA = 0.90). At perfect focus (Δz = 0 μm), the I_G profile exhibits a steep slope at x = 0 and the one for I_D, indeed, follows a Gaussian distribution. As Δz increases, the gradient of the I_G profile decreases, and the I_D profile broadens, indicating growth in both $R_{\Delta z}$ and LSR_{exp}. The derived LSR_{exp} from the I_G and I_D profiles are consistent with each other, and the average LSR_{exp} for Δz = 0, 0.3, and 0.6 μm are 0.35, 0.47, and 0.93 μm, respectively. While a defocus of 0.3 μm increases the LSR_{exp} by only ~0.1 μm, larger defocus misalignments lead to progressively stronger deviations. Therefore, proper laser focusing is essential to obtain a reliable LSR_{exp}.

Beyond the focus condition, effective utilization of the objective's NA is crucial for achieving optimal LSR_{exp}, which is quantified by the beam filling factor (δD_{LB}), i.e., the ratio of the laser beam diameter to the objective's entrance pupil diameter (e.g., 7 mm for the 50×, NA = 0.75 objective). Figure 5 displays the dependence of the I_G and I_D profiles near the 1LG edge for different δD_{LB}. When δD_{LB} = 1, the I_G profile shows a steep slope, while the one for I_D exhibits a Gaussian curve. Both the I_G profile gradient and I_D profile sharpness decrease with reducing δD_{LB}, leading to degraded LSR_{exp}. The experimental I_G and I_D profiles in Figs. 5(a)–5(c) are well fitted by Eqs. (4) and (5), respectively, with corresponding LSR_{exp} values are summarized in Table I. The deduced LSR_{exp} values from the I_G and I_D profiles are in good agreement with each other.

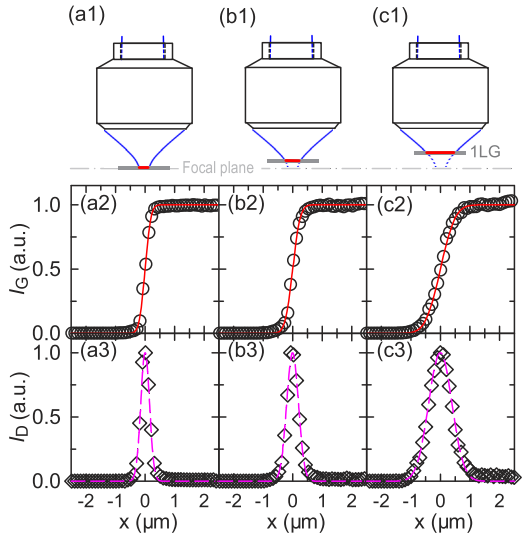

FIG. 4. Diagram of an objective (NA = 0.9) at different Δz values showing the focal plane and 1LG plane, with corresponding I_G and I_D as functions of edge distance: (a) Δz = 0 μm, (b) Δz = 0.3 μm, and (c) Δz = 0.6 μm, where the open circles/diamonds represent the experimental data and the solid/dashed lines correspond to the fitted results using Eqs. (4) and (5).

When the laser beam diameter is small, only the central portion of the lens is illuminated, reducing the effective collection angle of the focused beam. This results in an effective NA lower than the lens's nominal value,[41] degrading focusing performance and increasing the laser spot size. Conversely, expanding the beam to match the objective's entrance pupil diameter ensures full NA utilization, enabling tighter focusing and optimal LSR. These results underscore the critical need to match the laser beam diameter to the objective's entrance pupil for achieving the best LSR.

In principle, the D peak cannot be produced by a perfect zigzag edge, while it should appear near a perfect armchair edge.[38] For a perfect armchair edge, I_D should strongly depend on the angle between the incident polarization and the edge; it is maximum for polarization parallel to the edge and zero when perpendicular. However, in practice, I_D does not vanish for light polarized perpendicular to the edge because the edge is typically not perfectly armchair on a microscopic scale, even if it appears smooth under optical microscopy. Therefore, a perfect armchair edge is not strictly necessary for

TABLE I. Fitted LSR_{exp} values extracted from I_G and I_D edge-distance profiles using Eqs. (4) and (5), with corresponding theoretical LSR_{cf} calculated using Eq. (2), for objectives with varying NA, pinhole size, and beam filling factor (δD_{LB}).

NA		0.90	0.90	0.75	0.75	0.75	0.45	0.25
Pinhole size (μm)		20	80	80	80	80	80	80
δD_{LB}		1	1	1	0.43	0.14	1	1
LSR_{exp} (μm)	I_G	0.28 ± 0.01	0.37 ± 0.02	0.42 ± 0.01	0.65 ± 0.01	1.77 ± 0.04	0.72 ± 0.02	1.38 ± 0.05
	I_D	0.27 ± 0.01	0.35 ± 0.01	0.43 ± 0.01	0.64 ± 0.01	1.74 ± 0.01	0.71 ± 0.01	1.35 ± 0.01
LSR_{cf} (μm)		0.266	0.266	0.319	⋯	⋯	0.530	0.957

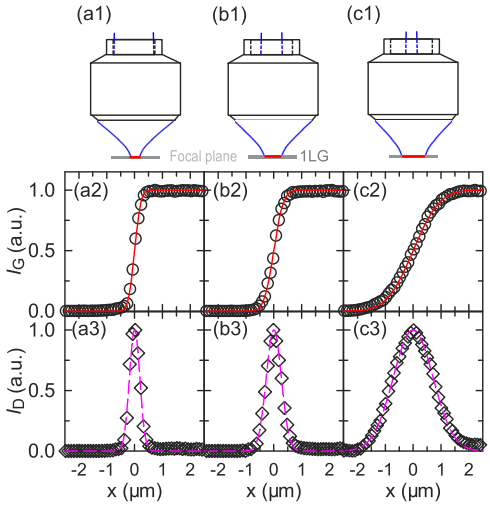

FIG. 5. Diagram of an objective (NA = 0.75) with different δD_{LB} values showing the focal plane and 1LG plane and the corresponding I_G and I_D as functions of edge distance: (a) δD_{LB} = 1, (b) δD_{LB} = 0.43, and (c) δD_{LB} = 0.14, where the open circles/diamonds represent the experimental data and the solid/dashed lines correspond to the fitted results using Eqs. (4) and (5).

cross-edge 1D Raman scan measurements as long as I_D at the edge is sufficiently strong to obtain LSR_{exp} by fitting the corresponding intensity profile. The D mode at the edge with intensity comparable to the G mode is unique to 1LG, making it an ideal sample for measuring LSR via two independent methods by fitting I_G and I_D with Eqs. (4) and (5), respectively.

V. CONCLUSION

In summary, we developed a method to determine the LSR of confocal Raman microscopy by analyzing the G and D mode intensities of 1LG near its edge through cross-edge 1D Raman scan measurements, where the edge-distance-dependent profiles of the G and D modes follow Sigmoid-like and Gaussian curves, respectively, with fitted LSR_{exp} values showing close agreement with diffraction-limited predictions for small pinhole size. Further investigations of pinhole size, focus depth, and beam diameter variations highlight the critical role of selection of pinhole size, proper focusing, and optimal beam expansion in achieving superior LSR. This approach, validated across multiple NAs, offers a practical and substrate-compatible framework for LSR assessment in confocal Raman microscopy.

ACKNOWLEDGMENTS

This work was supported by the National Key Research and Development Program of China (Grant No. 2023YFA1407000), the Strategic Priority Research Program of CAS (Grant No. XDB0460000), the National Natural Science Foundation of China (Grant Nos. 12322401, 12127807, and 12393832), Beijing Nova Program (Grant No. 20230484301), the Youth Innovation Promotion Association, Chinese Academy of Sciences (Grant No. 2023125), and the CAS Project for Young Scientists in Basic Research (Grant No. YSBR-026).

AUTHOR DECLARATIONS

Conflict of Interest

The authors have no conflicts to disclose.

Author Contributions

Z.-J.W. and T.L. contributed equally to this work.

Zhong-Jie Wang: Data curation (lead); Formal analysis (lead); Investigation (equal); Methodology (equal); Software (equal); Validation (equal); Visualization (equal); Writing – original draft (equal); Writing – review & editing (equal). **Tao Liu**: Data curation (lead); Formal analysis (lead); Investigation (equal); Methodology (equal); Software (equal); Validation (equal); Visualization (equal). **Xue-Lu Liu**: Data curation (equal); Investigation (equal). **Miao-Ling Lin**: Formal analysis (equal); Funding acquisition (equal); Investigation (equal); Methodology (equal); Resources (equal); Validation (equal); Visualization (equal); Writing – original draft (equal); Writing – review & editing (equal). **Ping-Heng Tan**: Conceptualization (lead); Data curation (equal); Formal analysis (equal); Funding acquisition (equal); Investigation (equal); Methodology (lead); Project administration (equal); Resources (equal); Supervision (lead); Validation (lead); Visualization (lead); Writing – original draft (lead); Writing – review & editing (lead).

DATA AVAILABILITY

The data that support the findings of this study are available from the corresponding author upon reasonable request.

REFERENCES

[1] A. Jorio, M. S. Dresselhaus, R. Saito, and G. F. Dresselhaus, *Raman Spectrocopy in graphene-related Systems* (Wiley-VCH, Weinheim, Germany, 2011).
[2] J.-B. Wu, M.-L. Lin, X. Cong, H.-N. Liu, and P.-H. Tan, "Raman spectroscopy of graphene-based materials and its applications in related devices," Chem. Soc. Rev. **47**, 1822–1873 (2018).
[3] E. Smith and G. Dent, *Modern Raman Spectroscopy: A Practical Approach* (John Wiley & Sons, Ltd., 2019).
[4] M. Glass and T. Dabbs, "The experimental effect of detector size on confocal lateral resolution," J. Microsc. **164**, 153–158 (1991).
[5] P. D. A. Pudney, T. M. Hancewicz, and D. G. Cunningham, "The use of confocal Raman spectroscopy to characterise the microstructure of complex biomaterials: Foods," J. Spectrosc. **16**, 217–225 (2002).
[6] G. G. Hoffmann, G. de With, and J. Loos, "Micro-Raman and tip-enhanced Raman spectroscopy of carbon allotropes," Macromol. Symp. **265**, 1–11 (2008).
[7] T. Wermelinger, S. A. Scott, M. G. Lagally, C. Hinderling, and R. Spoleank, "High lateral resolution analysis of stresses in silver thin films by means of Raman microscopy," AIP Conf. Proc. **1267**, 776–777 (2010).
[8] P. Verma, T. Ichimura, T. Yano, Y. Saito, and S. Kawata, "Nano-imaging through tip-enhanced Raman spectroscopy: Stepping beyond the classical limits," Laser Photonics Rev. **4**, 548–561 (2010).
[9] T. Schmid, N. Schäfer, S. Levcenko, T. Rissom, and D. Abou-Ras, "Orientation-distribution mapping of polycrystalline materials by Raman microspectroscopy," Sci. Rep. **5**, 18410 (2015).

[10]S. Mignuzzi, N. Kumar, B. Brennan, I. S. Gilmore, D. Richards, A. J. Pollard, and D. Roy, "Probing individual point defects in graphene via near-field Raman scattering," Nanoscale **7**, 19413–19418 (2015).
[11]F. Shao, W. Dai, Y. Zhang, W. Zhang, A. D. Schlüter, and R. Zenobi, "Chemical mapping of nanodefects within 2D covalent monolayers by tip-enhanced raman spectroscopy," ACS Nano **12**, 5021–5029 (2018).
[12]R. Basnet, C. Sun, H. Wu, H. T. Nguyen, F. E. Rougieux, and D. Macdonald, "Ring defects in n-type Czochralski-grown silicon: A high spatial resolution study using Fourier-transform infrared spectroscopy, micro-photoluminescence, and micro-Raman," J. Appl. Phys. **124**, 243101 (2018).
[13]Y. Fu, X. Ding, J. Li, and J. Zhang, "A novel knife-edge method for measuring the lateral resolution of confocal Raman microscopes," Proc. SPIE **11337**, 113370B (2019).
[14]Y. Kim, E. J. Lee, S. Roy, A. S. Sharbirin, L.-G. Ranz, T. Dieing, and J. Kim, "Measurement of lateral and axial resolution of confocal Raman microscope using dispersed carbon nanotubes and suspended graphene," Curr. Appl. Phys. **20**, 71–77 (2020).
[15]J. Park, J. Kim, and H. Kwon, "Evaluation of lateral resolution for confocal Raman microscopy using gold nano-lines made by electron beam lithography," Bull. Kor. Chem. Soc. **41**, 34–37 (2020).
[16]N. Itoh and N. Hanari, "Reliable evaluation of the lateral resolution of a confocal Raman microscope by using the tungsten-dot array certified reference material," Anal. Sci. **36**, 1009–1013 (2020).
[17]X. Ding, Y. Fu, F. Li, J. Zhang, and W. Liu, "An improved target method to quantitatively measure the lateral resolution of the confocal Raman microscope," J. Appl. Spectrosc. **87**, 1105–1111 (2021).
[18]A. Bereczki, J. Dipold, A. Z. Freitas, and N. U. Wetter, "Sub-10 nm nanoparticle detection using multi-technique-based micro-Raman spectroscopy," Polymers **15**, 4644 (2023).
[19]G. La Penna, C. Mancini, A. Proietti, L. Buccini, D. Passeri, N. Gambacorti, J. Richy, and M. Rossi, "Strained silicon technology: Non-destructive high-lateral-resolution characterization through tip-enhanced Raman spectroscopy," Appl. Spectrosc. **78**, 1245–1255 (2024).
[20]N. Itoh, "Comparison of lateral resolutions obtained by different methods for confocal Raman microscopes," J. Raman Spectrosc. **56**, 389–397 (2025).
[21]G. Kolhatkar, J. Plathier, and A. Ruediger, "Nanoscale investigation of materials, chemical reactions, and biological systems by tip enhanced Raman spectroscopy—A review," J. Mater. Chem. C **6**, 1307–1319 (2018).
[22]S. Jiang, Y. Zhang, R. Zhang, C. Hu, M. Liao, Y. Luo, J. Yang, Z. Dong, and J. G. Hou, "Distinguishing adjacent molecules on a surface using plasmon-enhanced Raman scattering," Nat. Nanotechnol. **10**, 865–869 (2015).
[23]M. M. Lucchese, F. Stavale, E. H. M. Ferreira, C. Vilani, M. V. O. Moutinho, R. B. Capaz, C. A. Achete, and A. Jorio, "Quantifying ion-induced defects and Raman relaxation length in graphene," Carbon **48**, 1592–1597 (2010).
[24]I. De Wolf, H. E. Maes, and S. K. Jones, "Stress measurements in silicon devices through Raman spectroscopy: Bridging the gap between theory and experiment," J. Appl. Phys. **79**, 7148–7156 (1996).
[25]J. M. Atkin, S. Berweger, A. C. Jones, and M. B. Raschke, "Nano-optical imaging and spectroscopy of order, phases, and domains in complex solids," Adv. Phys. **61**, 745–842 (2012).
[26]M. Kuball and J. W. Pomeroy, "A review of Raman thermography for electronic and opto-electronic device measurement with submicron spatial and nanosecond temporal resolution," IEEE Trans. Device Mater. Reliab. **16**, 667–684 (2016).
[27]M. Muller, *Introduction to Confocal Fluorescence Microscopy*, 2nd ed. (SPIE Press, Washington, 2006).
[28]M. S. Dresselhaus, G. Dresselhaus, A. Jorio, A. G. Souza Filho, M. A. Pimenta, and R. Saito, "Single nanotube Raman spectroscopy," Acc. Chem. Res. **35**, 1070–1078 (2002).
[29]Y. Suzaki and A. Tachibana, "Measurement of the μm sized radius of Gaussian laser beam using the scanning knife-edge," Appl. Opt. **14**, 2809–2810 (1975).
[30]P. Hauer, J. Grand, A. Djorovic, G. R. Willmott, and E. C. Le Ru, "Spot size engineering in microscope-based laser spectroscopy," J. Phys. Chem. C **120**, 21104–21113 (2016).
[31]T. Liu, M.-L. Lin, D. Meng, X. Cong, Q. Kan, J.-B. Wu, and P.-H. Tan, "Intensity enhancement of Raman active and forbidden modes induced by naturally occurred hot spot at GaAs edge," Chin. Phys. B **34**, 17801–017801 (2024).
[32]M. Khorasaninejad, J. Walia, and S. S. Saini, "Enhanced Raman scattering from sub-wavelength silicon gratings," Appl. Phys. Lett. **103**, 163110 (2013).
[33]V. Poborchii, T. Tada, and T. Kanayama, "Edge-enhanced Raman scattering in Si nanostripes," Appl. Phys. Lett. **94**, 131907 (2009).
[34]X. Chen, M.-L. Lin, X. Cong, Y.-C. Leng, X. Zhang, and P.-H. Tan, "Intrinsic phonon anharmonicity in heavily doped graphene probed by Raman spectroscopy," Carbon **185**, 282–288 (2021).
[35]R. S. Quimby, "Gaussian beam optics," in *Photonics and Lasers* (John Wiley & Sons, Ltd., 2006), Chap. 17, pp. 307–325.
[36]International Organization for Standardization (ISO), Surface Chemical Analysis—Determination of Lateral Resolution and Sharpness in Beam Based Methods With a Range From Nanometres to Micrometres, ISO 18516:2019 ed., International Organization for Standardization, Geneva, 2019.
[37]A. C. Ferrari, J. C. Meyer, V. Scardaci, C. Casiraghi, M. Lazzeri, F. Mauri, S. Piscanec, D. Jiang, K. S. Novoselov, S. Roth, and A. K. Geim, "Raman spectrum of graphene and graphene layers," Phys. Rev. Lett. **97**, 187401 (2006).
[38]C. Casiraghi, A. Hartschuh, H. Qian, S. Piscanec, C. Georgi, A. Fasoli, K. S. Novoselov, D. M. Basko, and A. C. Ferrari, "Raman spectroscopy of graphene edges," Nano Lett. **9**, 1433–1441 (2009).
[39]X.-L. Liu, X. Zhang, M.-L. Lin, and P.-H. Tan, "Different angle-resolved polarization configurations of Raman spectroscopy: A case on the basal and edge plane of two-dimensional materials," Chin. Phys. B **26**, 067802 (2017).
[40]P. H. Tan, Z. Y. Xu, X. D. Luo, W. K. Ge, Y. Zhang, A. Mascarenhas, H. P. Xin, and C. W. Tu, "Resonant Raman scattering with the E_+ band in a dilute $GaAs_{1-x}N_x$ alloy (x = 0.1%)," Appl. Phys. Lett. **89**, 101912 (2006).
[41]Total internal reflection fluorescence microscopy," in *Optical Imaging and Microscopy: Techniques and Advanced Systems*, edited by P. Török and F.-J. Kao (Springer, Berlin, Heidelberg, 2007), pp. 195–236.